Ocean Engineering 195 (2020) 106711

Contents lists available at ScienceDirect

Ocean Engineering

journal homepage: www.elsevier.com/locate/oceaneng

An analytical investigation of oscillations within a circular harbor over a Conical Island

Gang Wang [a], Ze Eyezo'o Giresse Stanis [a], Danjuan Fu [b], Jinhai Zheng [a,*], Junliang Gao [c]

[a] Key Laboratory of Coastal Disaster and Defense (Hohai University), Ministry of Education, Nanjing, 210098, China
[b] School of Civil Engineering & Architecture, Xiamen University of Technology, Xiamen, 361024, China
[c] School of Naval Architecture and Ocean Engineering, Jiangsu University of Science and Technology, Zhenjiang, 212003, China

ARTICLE INFO

Keywords:
Harbor resonance
Wave oscillations
Circular harbor
Conical island
Analytical solution

ABSTRACT

Based on the linearized long-wave equation, an analytical solution for wave oscillations within a circular harbor of constant depth over a conical island is obtained. The analysis divides the study domain into three regions: region I (within the harbor), region II (over the island) and region III (from the island toe to the deep sea). In region I, the water depth is uniform, and the method of separation of variables is used to find the free-surface elevation solution. In Region II, the water depth linearly varies along the radial direction of the island, and the method of separation of variables is adopted again to reveal the free-surface elevation solution expressed in Bessel and Hankel functions. Waves in region III consist of the incident waves and the scattered waves from the island, which are respectively expressed with a Fourier-cosine series and a sum series of Hankel function. The final solution is obtained by matching the free-surface elevation and its normal derivatives at the interfaces between the three regions. To confirm the validity of the analytical solution, via adjusting topographical parameters, it was further utilized to compare with the existing analytical solutions for wave-induced oscillations in a circular harbor of constant depth and the scattering of long waves around a cylindrical island mounted on a conical shoal. Finally, as the topographical features of Maug Islands resembles the geometry studied in this article, the coupled oscillation characteristics for Maug Islands are examined. The existence of the island does aggravate oscillations within the harbor, and the features are addressed in details.

1. Introduction

Among the natural disasters related to long-period waves, harbor oscillations are one of the most frequent disasters around the world. Long period oscillations associated with resonance can cause excessive movements of moored ships, break ships mooring lines and interrupt normal operation of the harbor (Gao et al., 2017). Therefore, it is of paramount importance to predict accurately the response of a newly designed harbor to incident long-period waves from the high sea. The issue of harbor oscillations had been extensively addressed, including the generation mechanisms and the factors involving in amplification of waves in harbors and bays. Tsunamis were regarded as one of the common factors exciting larger oscillations in bays, inlets, and harbors (Dong et al., 2010a; Vela et al., 2014). The term tsunami comes from the Japanese term with the literal meaning of harbor wave, which may reflect the fact that tsunami waves were first observed in harbors. Historic records of unexplained and rapid rises of water level in harbors can go back almost 1000 years in Japan, and they are often associated with tsunamis (Synolakis, 2003). Atmospheric disturbances such as atmospheric gravity waves, pressure jumps, frontal passages, squalls can also generate long waves with the same temporal and spatial scales as typical tsunami waves, known as meteotsunamis (Ličer et al., 2017). These meteotsunami waves will be resonant amplificated when they arrive at the harbor entrance (Wijeratne et al., 2010). Furthermore, long waves generated through the nonlinear interaction of wind waves or swell termed infragravity waves can also be responsible for harbor. Oscillations with typical periods of several minutes present at all times but increasing significantly during storm events commonly arise from infragravity waves incident on the harbor entrance (Thotagamuwage and Pattiaratchi, 2014; Dong et al., 2010b).

Oscillations within bays and harbors depend not only on the characteristics of incident long waves but also on the geometrical features. To reveal the influence of the harbor geometry on the amplification of wave oscillation, Miles and Munk (1961), Lee (1971) and Marcos et al.

* Corresponding author.
E-mail addresses: gangwang@hhu.edu.cn (G. Wang), jhzheng@hhu.edu.cn (J. Zheng).

https://doi.org/10.1016/j.oceaneng.2019.106711
Received 20 July 2019; Received in revised form 3 October 2019; Accepted 10 November 2019
Available online 21 November 2019

(2005) formulated analytical solutions for simple geometries of uniform water depth within and outside the harbor. Zelt and Raichlen (1990), Wang et al. (2011a) and Wang et al. (2014) have provided analytical solutions for wave-induced oscillations in harbors of variable bathymetries. These analytical solutions can help to understand some general properties of oscillations. However, the geometric shapes and depth profiles for real harbors are more complex and they must yield more complicated oscillations, which significantly increases the difficulty in carrying out the theoretical investigation. Therefore, a number of numerical models have been developed to handle oscillations in harbors of complex shapes and bathymetries. Lee et al. (1998) adopted the finite element model of the mild-slope equation to study resonance in Long Beach and Los Angeles harbor basins. Losada et al. (2008) presented a Boussinesq model based on a finite element unstructured grid to analyze transient nonlinear resonance problems in harbors and bays. Wang et al. (2011b) developed a Boussinesq model to simulate harbor oscillations induced by seafloor movements. Kumar et al. (2013) proposed a boundary element model based on the Helmholtz equation and implemented investigations on the Pohang New Harbor to predict the resonance modes for incident waves with various directions. Cuomo and Guza (2017) proposed a method to estimate harbor oscillations with infragravity periods at Marina di Carrara from the properties of wind-generated incident waves outside the harbor.

Previous studies on harbor oscillations mostly focus on harbors located on the coastline of the mainland. However, there are quite a number of harbors built over natural or artificial islands. When long waves approach water of variable depth, they may be greatly amplified by the island. Therefore, it is imperative to further examine the response of a harbor over an island. Solutions for the problem of waves scattering on islands are mostly based on the shallow water equation and the mild-slope equation. Wave amplification around the island depends on the trapping capability of the island, and how factors such as wave periods, radii of the island and depth-varying parameters etc. affect the response characteristics of the island to long waves has been widely examined (Jung et al., 2010; Liu and Xie, 2013; Wang et al., 2018; Zhang and Zhu, 1994; Zhu and Zhang, 1996).

Maug islands with the coordinate of (20°2′N, 145°13′E) are a group of three small uninhabited islands in the Commonwealth of the Northern Mariana Island. This island group was formed as a result of a volcano that broke through the Pacific Ocean. The three islands have a total area of approximately 2.1 km^2 and a maximum elevation of 227 m. The submerged caldera has a diameter of approximately 2.2 km. The floor of the caldera is around 225 m below sea level, and in the middle is a mountain whose summit is only 22 m below sea level. As the caldera is protected by the three islands with a gap southward, it can be considered as a natural harbor for ship docking. As the incident waves will be coordinately responded by the islands and the harbor, it is motivated to examine the coupled oscillation characteristics for this new configuration.

Although harbor resonance and wave amplification around islands have been widely explored independently, the recognized phenomenon of violent oscillations in a coupled harbor-island system still lacks a rigorous theory to provide detailed characteristics. In this paper, we proposed an analytical model to reveal the interesting features not emerged in the decoupled system. The present study restricts the analysis to a circular harbor with constant water depth over a conical island, so that the analytical solution can be explicitly obtained. The study further makes a further simplifying assumption that the mouth width is small as compared to the wavelength of interest, and deduce the analytical solution in Section 2. The deduced analytical solution is verified by applying it to the oscillations within a circular harbor of constant water depth and the response of the conical island to long waves in Section 3. Oscillations within the circular harbor over Maug Islands are then investigated analytically, and the impact of the islands on the response of the harbor is addressed in details in Section 4. Conclusions are drawn in Section 5.

2. Analytical solution

Maug Islands can be simplified as a circular harbor over a conical island as illustrated in Fig. 2. The interesting domain is divided into region I, region II and region III, which are respectively the regions within the harbor, over the island and the open sea. Water depth within the harbor and in the open sea keeps constant as h_1 and h_2, respectively. Whilst in region II, the water depth varies with a constant slope s. Therefore, the water depth in the whole domain can be expressed as

$$h=\begin{cases} h_1 0 \le r \le r_1 \\ s r r_1 < r \le r_2 \\ h_2 r > r_2 \end{cases}, \tag{1}$$

where $h_1 = sr_1$ and $h_2 = sr_2$, and r_1 and r_2 are the radial distances from the center to the coastline and the island toe, respectively.

It is customary and appropriate to use the linear shallow-water equation in harbor oscillation studies (Synolakis, 2003). For oscillations in a circular basin and wave propagation over a conical island, it is convenient to use a polar coordinate system (r, θ) with the origin in the center. Using the expression of the free-surface elevation $\eta(r, \theta, t) = \zeta(r, \theta)\exp(i\sigma t)$, the linearized long wave equation can be written as

$$r^2\frac{\partial^2\zeta}{\partial r^2}+r\left(1+\frac{r}{h}\frac{\partial h}{\partial r}\right)\frac{\partial\zeta}{\partial r}+\frac{\partial^2\zeta}{\partial\theta^2}+\frac{\sigma^2 r^2}{gh}\zeta=0\ . \tag{2}$$

2.1. In region I (within the harbor)

As the water depth within the harbor is constant, Eq.(2) can be reduced to

$$r^2\frac{\partial^2\zeta}{\partial r^2}+r\frac{\partial\zeta}{\partial r}+\frac{\partial^2\zeta}{\partial\theta^2}+\frac{\sigma^2 r^2}{gh}\zeta=0\ . \tag{3}$$

Considering that waves propagate at $\theta = 0$ or $\theta = \pi$ respectively, so the wave amplitude should be symmetrical with respect to the center line $\theta = 0$, thus the solution of Eq. (3) can be expressed as

$$\zeta_1(r,\theta)=\sum_{n=0}^{\infty}A_I^n \mathrm{J}_n(k_1 r)\cos n\theta\ , \tag{4}$$

where $\mathrm{J_n}$ is the first kind Bessel function of the nth order, $k_1 = \sigma/\sqrt{gh_1}$ is the wavenumber and A_I^n is an arbitrary constant to be determined by matching the conditions at the interface of $r = r_1$ as follows:

$$\left.\frac{\partial\zeta_1}{\partial r}\right|_{r=r_1}=\begin{cases} F(\theta) & |\theta|\le\theta_0 \\ 0 & |\theta|>\theta_0 \end{cases}\ . \tag{5}$$

There are relationships for the Bessel functions

$$\frac{\partial \mathrm{J}_0(kr)}{\partial r}=-k\cdot\mathrm{J}_1(kr)\ , \tag{6}$$

and

$$\frac{\partial \mathrm{J}_n(kr)}{\partial r}=k\cdot\mathrm{J}_{n-1}(kr)-\frac{n}{r}\mathrm{J}_n(kr)\qquad n\ge 1\ . \tag{7}$$

Thus, the matching conditions Eq. (5) can then be expressed as

$$\left.\frac{\partial\zeta_1}{\partial r}\right|_{r=r1}=-k_1\cdot A_I^0\cdot\mathrm{J}_1(k_1 r_1)+\ \backslash$$
$$\sum_{n=1}^{\infty}A_I^n\left[k_1\cdot\mathrm{J}_{n-1}(k_1 r_1)-\frac{n}{r_1}\mathrm{J}_n(k_1 r_1)\right]\cos n\theta=\begin{cases} F(\theta) & |\theta|\le\theta_0 \\ 0 & |\theta|>\theta_0 \end{cases}. \tag{8}$$

Multiplying Eq.(8) by cos(n'θ) (where n' is integer) and integrating it with respect to θ from 0 to 2π leads to

$$-k_1 \cdot A_I^0 \cdot \mathrm{J}_1(k_1 r_1) \int_0^{2\pi} \cos n' \theta \mathrm{d}\theta +$$

$$\int_0^{2\pi} \sum_{n=1}^{\infty} A_I^n \left[k_1 \cdot \mathrm{J}_{n-1}(k_1 r_1) - \frac{n}{r_1} \mathrm{J}_n(k_1 r_1) \right] \cos n\theta \cos n' \theta \mathrm{d}\theta \tag{9}$$

$$= \int_{-\theta_0}^{\theta_0} F(\theta) \cos n' \theta \mathrm{d}\theta \ .$$

Setting $n' = 0$, $A^0{}_{\mathrm{I}}$ can be determined as

$$A_I^0 = -\frac{1}{2\pi k_1 \cdot \mathrm{J}_1(k_1 r_1)} \int_{-\theta_0}^{\theta_0} F(\theta) \mathrm{d}\theta \ . \tag{10}$$

On the other hand, if $n' = n \neq 0$, $A^n{}_{\mathrm{I}}$ can be evaluated as

$$A_I^n = \frac{\int_{-\theta_0}^{\theta_0} F(\theta) \cos n\theta \mathrm{d}\theta}{\pi \left[k_1 \cdot \mathrm{J}_{n-1}(k_1 r_1) - \frac{n}{r_1} \mathrm{J}_n(k_1 r_1) \right]} \quad n \geq 1 \ . \tag{11}$$

This above formula is formally the same as that for the circular harbor derived by Lee (1971), and $F(\theta)$ can be approximated by a constant F if the harbor entrance is assumed very small compared to the wavelength. Hence Eqs. (10) and (11) can be transformed to

$$A_I^n = \begin{cases} -\dfrac{\theta_0 F}{\pi k_1 \cdot \mathrm{J}_1(k_1 r_1)} & n = 0 \\ \dfrac{2 \sin n\theta_0 F}{\pi n \left[k_1 \cdot \mathrm{J}_{n-1}(k_1 r_1) - \frac{n}{r_1} \mathrm{J}_n(k_1 r_1) \right]} & n \geq 1 \end{cases} . \tag{12}$$

2.2. In region II (over the island)

Over the island, the wave system consists of incident waves from the open sea, reflected wave by the harbor wall and radiated waves from the harbor entrance. Separating the variable as $\zeta(r, \theta) = R(r) \cdot \Theta(\theta)$ and inserting the expression of the bathymetry (1) into Eq.(2) yield

$$R'' + \frac{2}{r} R' + \left[\frac{\sigma^2}{gsr} - \frac{n^2}{r^2} \right] R = 0 \ , \tag{13}$$

and

$$\Theta'' + n^2 \Theta = 0 \ . \tag{14}$$

As the island is symmetrical with respect to the center line $\theta = 0$, the solution of Eq.(14) is

$$\Theta(\theta) = A_{\mathrm{II}}^{'n} \cdot \cos(n\theta) \ , \tag{15}$$

where $A_{\mathrm{II}}^{'n}$ is an arbitrary constant.

Introducing

$$\tau = \frac{2\sigma}{\sqrt{gs}} r^{\frac{1}{2}} \ , \tag{16}$$

and

$$R = r^{-\frac{1}{2}} \mathbb{R} \ , \tag{17}$$

Eq.(13) becomes

$$\frac{\partial^2 \mathbb{R}}{\partial \tau^2} + \tau^{-1} \frac{\partial \mathbb{R}}{\partial \tau} + \left[1 - \nu^2 \tau^{-2} \right] \mathbb{R} = 0 \ , \tag{18}$$

where

$$\nu = \sqrt{4n^2 + 1} \ . \tag{19}$$

Eq.(18) is the Bessel equation of order ν, and its corresponding solution can be expressed as

$$\mathbb{R} = A_{\mathrm{II}} \cdot \mathrm{J}_\nu(\tau) + B_{\mathrm{II}} \cdot \mathrm{Y}_\nu(\tau) \ , \tag{20}$$

where J_ν and Y_ν are the ν^{th} order Bessel functions of the first and second kinds, respectively, and A^{II} and B^{II} are constants, which can be obtained from the boundary condition and matching relations.

There are the radiated waves from the harbor entrance, each point (x', y') can be considered as a source, and the waves scattered from it can be expressed as

$$\zeta_{\mathrm{II}}^{\mathrm{rd}}(x', y') = \frac{\sigma \cdot G(x', y')}{2g} \cdot H_0^{(1)}(k_1 r') \ , \tag{21}$$

where G (x', y') is the flow of the point (x', y'), $\mathrm{H}_0^{(1)}$ is the 0^{th} order Hankel function of the first kind and $r'^2 = (x - x')^2 + (y - y')^2$. The total radiated waves can be written as

$$\zeta_{\mathrm{II}}^{\mathrm{rd}} = \int_{-\theta_0}^{\theta_0} \frac{\sigma \cdot G(x', y')}{2g} \mathrm{H}_0^{(1)}(k_1 r') \cdot r_1 \mathrm{d}\theta' \ . \tag{22}$$

According to Wang et al. (2011a), $G(x', y')$ can be approximated as a constant G if the harbor entrance is assumed narrow. The arc from $-\theta_0$ to θ_0 can be further approximated as a straight-line segment. Thus, the radiated waves at the entrance can be approximated as

$$\zeta_{\mathrm{II}}^{\mathrm{rd}} \approx \frac{\sigma \cdot G}{2g} \int_{-r_1 \sin\theta_0}^{r_1 \sin\theta_0} H_0^{(1)} \left(k_1 \sqrt{(x - x')^2 + (y - y')^2} \right) \cdot \mathrm{d}y' \tag{23}$$

So, the wave field over the island is described by

$$\zeta_{\mathrm{II}} = \sum_{n=0}^{\infty} r^{-\frac{1}{2}} \left\{ A_{\mathrm{II}}^n \cdot \mathrm{J}_\nu \left[2\sigma (gs)^{-\frac{1}{2}} r^{\frac{1}{2}} \right] + B_{\mathrm{II}}^n \cdot \mathrm{Y}_\nu \left[2\sigma (gs)^{-\frac{1}{2}} r^{\frac{1}{2}} \right] \right\} \cdot \cos(n\theta)$$
$$+ \frac{\sigma \cdot G}{2g} \int_{-r_1 \sin\theta_0}^{r_1 \sin\theta_0} H_0^{(1)} \left(k_1 \sqrt{(x - x')^2 + (y - y')^2} \right) \cdot \mathrm{d}y' \tag{24}$$

2.3. In region III (the open sea)

There are incident waves from the open sea $\zeta_{\mathrm{III}}{}^{\mathrm{I}}(r, \theta)$ and scattered waves by the island $\zeta_{\mathrm{III}}{}^{\mathrm{s}}(r, \theta)$. The water surface elevation $\zeta_{\mathrm{III}}(r, \theta)$ may be expressed as

$$\zeta_{\mathrm{III}}(r, \theta) = \zeta_{\mathrm{III}}^{\mathrm{I}}(r, \theta) + \zeta_{\mathrm{III}}^{\mathrm{s}}(r, \theta) \ . \tag{25}$$

The incident waves are assumed to be a linear sinusoidal wave train propagating in the positive x direction, which can be expressed in terms of Fourier-cosine series as (Synolakis, 2003),

$$\zeta_{\mathrm{III}}^I(r, \theta) = a_{\mathrm{I}} e^{ik_2 x} = a_{\mathrm{I}} \sum_{n=0}^{\infty} \mathrm{i}^n \varepsilon_n \mathrm{J}_n(k_2 r) \cos n\theta \ , \tag{26}$$

where a_{I} is the incident wave amplitude, $k_2 = \sigma / \sqrt{gh_2}$ is the wavenumber, ε_n is the Jacobi symbol defined by

$$\varepsilon_n = \begin{cases} 1, n = 0 \\ 2, n \geq 1 \end{cases} . \tag{27}$$

The scattered wave may be expressed as (Wang et al., 2014)

$$\zeta_{\mathrm{III}}^s(r, \theta) = \sum_{n=0}^{\infty} a_{\mathrm{III}}^n \mathrm{H}_n(k_2 r) \cos n\theta \ , \tag{28}$$

where a_n^{III} is the scattered wave amplitude to be determined, H_n is the nth order Hankel function of the first kind. The free-surface elevation in the outer region can finally be obtained:

$$\zeta_{\mathrm{III}}(r, \theta) = a_{\mathrm{I}} \sum_{n=0}^{\infty} \mathrm{i}^n \varepsilon_n \mathrm{J}_n(k_2 r) \cos n\theta + \sum_{n=0}^{\infty} a_{\mathrm{III}}^n \mathrm{H}_n(k_2 r) \cos n\theta \ . \tag{29}$$

2.4. Matching and boundary conditions

The free-surface elevation and its derivative should be continuous at $r = r_1$ ($|\theta| \le \theta_0$). Hence,

$$\zeta_{\mathrm{I}} = \zeta_{\mathrm{II}} \qquad |\theta| \le \theta_0 \ , \tag{30}$$

and

$$\left.\frac{\partial \zeta_{\mathrm{II}}}{\partial r}\right|_{r=r_1} = \begin{cases} 0 & |\theta| > \theta_0 \\ \left.\dfrac{\partial \zeta_{\mathrm{I}}}{\partial r}\right|_{r=r_1} & |\theta| \le \theta_0 \end{cases} . \tag{31}$$

Similarly, the free-surface elevation and its derivative should be continuous at $r = r_2$, which requires

$$\zeta_{\mathrm{III}}|_{r=r_2} = \zeta_{\mathrm{II}}|_{r=r_2} \ , \tag{32}$$

and

$$\left.\frac{\partial \zeta_{\mathrm{III}}}{\partial r}\right|_{r=r_2} = \left.\frac{\partial \zeta_{\mathrm{II}}}{\partial r}\right|_{r=r_2} . \tag{33}$$

The matching condition (32) implies that

$$\left.\frac{\partial \zeta_{\mathrm{II}}^{\mathrm{rd}}}{\partial r}\right|_{r=r_1} = \left.\frac{\partial \zeta_{\mathrm{I}}}{\partial r}\right|_{r=r_1} \quad \text{for} \quad |\theta| \le \theta_0 \ . \tag{34}$$

For the narrow entrance, the matching condition Eq. (34) can be changed to

$$\int_{-\theta_0}^{\theta_0} \left.\frac{\partial \zeta_{\mathrm{II}}^{\mathrm{rd}}}{\partial r}\right|_{r=r_1} r_1 \mathrm{d}\theta = \int_{-\theta_0}^{\theta_0} \left.\frac{\partial \zeta_{\mathrm{I}}}{\partial r}\right|_{r=r_1} r_1 \mathrm{d}\theta \ , \tag{35}$$

which yields

$$\frac{\sigma \cdot G}{2g} \int_{-\theta_0}^{\theta_0} \left\{ \frac{\partial}{\partial r} \left[\int_{-r_1 \sin\theta_0}^{r_1 \sin\theta_0} H_0^{(1)}\left(k_1 \sqrt{(x-x')^2 + (y-y')^2}\right) \cdot \mathrm{d}y' \right] \Big|_{r=r_1} \right\} r_1 \mathrm{d}\theta$$

$$= -2\theta_0 k_1 r_1 A_0^1 \mathrm{J}_1(k_1 r_1) + k_1 r_1 \sum_{n=1}^{\infty} \frac{\sin n\theta_0}{n} A_n^1 [\mathrm{J}_{n-1}(k_1 r_1) - \mathrm{J}_{n+1}(k_1 r_1)] \ . \tag{36}$$

If the integral along the arc can be approximated as if it is along a straight-line segment, the derivative of r can be approximated as that of x. Thus, Eq. (36) becomes

$$\frac{\sigma \cdot G}{2g} \int_{-r_1 \sin\theta_0}^{r_1 \sin\theta_0} \left\{ \left[\int_{-r_1 \sin\theta_0}^{r_1 \sin\theta_0} \frac{\partial}{\partial x} H_0^{(1)}\left(k_1 \sqrt{(x-x')^2 + (y-y')^2}\right) \cdot \mathrm{d}y' \right] \Big|_{r=r_1} \right\} \mathrm{d}y$$

$$= -2\theta_0 k_1 r_1 A_0^1 \mathrm{J}_1(k_1 r_1) + k_1 r_1 \sum_{n=1}^{\infty} \frac{\sin n\theta_0}{n} A_n^1 [\mathrm{J}_{n-1}(k_1 r_1) - \mathrm{J}_{n+1}(k_1 r_1)] \ . \tag{37}$$

For $kr \ll 1$, $\mathrm{H}_0^{(1)}(kr)$ can be extended asymptotically as (Wang et al., 2011a)

$$H_0^{(1)}(kr) = 1 + \frac{2\mathrm{i}}{\pi} \ln\left(\frac{\gamma kr}{2}\right) + O(kr)^2 \ , \tag{38}$$

where $\gamma = 1.7810724$ is the exponential of Euler's constant.

Inserting Eq.(38) into Eq.(37) yields

$$\frac{\mathrm{i}\sigma \cdot G}{g\pi} \int_{-r_1 \sin\theta_0}^{r_1 \sin\theta_0} \int_{-r_1 \sin\theta_0}^{r_1 \sin\theta_0} \frac{x - x'}{(x-x')^2 + (y-y')^2} \cdot \mathrm{d}y' \mathrm{d}y =$$

$$-2\theta_0 k_1 r_1 A_0^1 \mathrm{J}_1(k_1 r_1) + k_1 r_1 \sum_{n=1}^{\infty} \frac{\sin n\theta_0}{n} A_n^1 [\mathrm{J}_{n-1}(k_1 r_1) - \mathrm{J}_{n+1}(k_1 r_1)] \tag{39}$$

$$(x - x' \to 0^+, |y| \le r_1 \sin\theta_0) \ .$$

Notice that when $x - x' \to 0^+$, the integral in Eq.(39) takes the algebraic form

$$\int_{-r_1 \sin\theta_0}^{r_1 \sin\theta_0} \frac{x - x'}{(x-x')^2 + (y-y')^2} \cdot \mathrm{d}y'$$

$$\approx \int_{y-\delta}^{y+\delta} \frac{x - x'}{(x-x')^2 + (y-y')^2} \cdot \mathrm{d}y' \tag{40}$$

$$= \arctan \left. \frac{y - y'}{x - x'} \right|_{y-\delta}^{y+\delta} = \pi \ .$$

Substituting Eq.(40) into Eq.(39) leads to

$$G = \frac{\mathrm{i}g\theta_0 k_1 A_0^1}{\sigma \cdot \sin\theta_0} \mathrm{J}_1(k_1 r_1) - \frac{\mathrm{i}g k_1}{\sigma \cdot \sin\theta_0} \sum_{n=1}^{\infty} \frac{\sin n\theta_0}{2n} A_n^1 [\mathrm{J}_{n-1}(k_1 r_1) - \mathrm{J}_{n+1}(k_1 r_1)] \ . \tag{41}$$

The radiated waves from the harbor are assumed to be limited near the narrow mouth, and they can be neglected at $|\theta| > \theta_0$. Thus, the matching condition Eq.(31) can be changed to

$$\frac{\partial}{\partial r} \sum_{n=0}^{\infty} r^{-\frac{1}{2}} \cos(n\theta) \left\{ A_{\mathrm{II}}^n \mathrm{J}_\nu \left[2\sigma(gs)^{-\frac{1}{2}} r^{\frac{1}{2}} \right] + B_{\mathrm{II}}^n \mathrm{Y}_\nu \left[2\sigma(gs)^{-\frac{1}{2}} r^{\frac{1}{2}} \right] \right\} \Big|_{r=r_1} = 0 \ , \tag{42}$$

which yields

$$-A_{\mathrm{II}}^n \cdot \mathrm{J}_\nu \left[2\sigma(gs)^{-\frac{1}{2}} r_1^{\frac{1}{2}} \right] - B_{\mathrm{II}}^n \cdot \mathrm{Y}_\nu \left[2\sigma(gs)^{-\frac{1}{2}} r_1^{\frac{1}{2}} \right] +$$

$$\sigma(gs)^{-\frac{1}{2}} r_1^{\frac{1}{2}} \left\{ \begin{array}{l} A_{\mathrm{II}}^n \cdot \left\{ \mathrm{J}_{\nu-1} \left[2\sigma(gs)^{-\frac{1}{2}} r_1^{\frac{1}{2}} \right] - \mathrm{J}_{\nu+1} \left[2\sigma(gs)^{-\frac{1}{2}} r_1^{\frac{1}{2}} \right] \right\} \\ + B_{\mathrm{II}}^n \cdot \left\{ \mathrm{Y}_{\nu-1} \left[2\sigma(gs)^{-\frac{1}{2}} r_1^{\frac{1}{2}} \right] - \mathrm{Y}_{\nu+1} \left[2\sigma(gs)^{-\frac{1}{2}} r_1^{\frac{1}{2}} \right] \right\} \end{array} \right\} = 0 \ . \tag{43}$$

The matching condition Eq.(30) can be changed to

$$\int_{-\theta_0}^{\theta_0} \zeta_{\mathrm{II}} r_1 \mathrm{d}\theta = \int_{-\theta_0}^{\theta_0} \zeta_{\mathrm{I}} r_1 \mathrm{d}\theta \ , \tag{44}$$

or

$$2\theta_0 r_1^{-\frac{1}{2}} \left\{ A_{II}^0 \cdot \mathrm{J}_\nu \left[2\sigma(gs)^{-\frac{1}{2}} r_1^{\frac{1}{2}} \right] + B_{II}^0 \cdot \mathrm{Y}_\nu \left[2\sigma(gs)^{-\frac{1}{2}} r_1^{\frac{1}{2}} \right] \right\} +$$

$$2 \sum_{n=1}^{\infty} r_1^{-\frac{1}{2}} \left\{ A_{II}^n \cdot \mathrm{J}_\nu \left[2\sigma(gs)^{-\frac{1}{2}} r_1^{\frac{1}{2}} \right] + B_{II}^n \cdot \mathrm{Y}_\nu \left[2\sigma(gs)^{-\frac{1}{2}} r_1^{\frac{1}{2}} \right] \right\} \cdot \frac{\sin(n\theta_0)}{n} \tag{45}$$

$$+ \frac{\sigma \cdot G}{2g} \int_{-\theta_0}^{\theta_0} \int_{-r_1 \sin\theta_0}^{r_1 \sin\theta_0} H_0^{(1)}\left(k_1 \sqrt{(x-x')^2 + (y-y')^2}\right) \cdot \mathrm{d}y' \mathrm{d}\theta$$

$$= 2\theta_0 A_0^1 \mathrm{J}_0(k_1 r_1) + \sum_{m=1}^{\infty} \frac{2 \sin n\theta_0}{n} A_n^1 \mathrm{J}_n(k_1 r_1) \ .$$

Using again the integral across a straight line to approximate the integral along the arc, Eq.(45) becomes

$$2\theta_0 r_1^{-\frac{1}{2}}\left\{A_{II}^0\cdot \mathrm{J}_\nu\left[2\sigma(gs)^{-\frac{1}{2}}r_1^{\frac{1}{2}}\right]+B_{II}^0\cdot \mathrm{Y}_\nu\left[2\sigma(gs)^{-\frac{1}{2}}r_1^{\frac{1}{2}}\right]\right\}+$$

$$2\sum_{n=1}^{\infty} r_1^{-\frac{1}{2}}\left\{A_{II}^n\cdot \mathrm{J}_\nu\left[2\sigma(gs)^{-\frac{1}{2}}r_1^{\frac{1}{2}}\right]+B_{II}^n\cdot \mathrm{Y}_\nu\left[2\sigma(gs)^{-\frac{1}{2}}r_1^{\frac{1}{2}}\right]\right\}\cdot\frac{\sin(n\theta_0)}{n} \tag{46}$$

$$+\frac{\sigma\cdot G}{2gr_1}\int_{-r_1\ \sin\theta_0}^{r_1\ \sin\theta_0}\int_{-r_1\ \sin\theta_0}^{r_1\ \sin\theta_0} H_0^{(1)}\left(k_1\sqrt{(x-x')^2+(y-y')^2}\right)\cdot \mathrm{d}y'\mathrm{d}y$$

$$=2\theta_0 A_0^1 \mathrm{J}_0(k_1r_1)+\sum_{m=1}^{\infty}\frac{2\sin n\theta_0}{n}A_n^1\mathrm{J}_n(k_1r_1)\quad .$$

Using the approximation Eq.(38) to substitute the Hankel function term in Eq.(46), we obtain

$$\int_{-r_1\ \sin\theta_0}^{r_1\ \sin\theta_0}\int_{-r_1\ \sin\theta_0}^{r_1\ \sin\theta_0} H_0^{(1)}\left(k_1\sqrt{(x-x')^2+(y-y')^2}\right)\cdot \mathrm{d}y'\mathrm{d}y$$

$$=4\int_0^{\sqrt{2}r_1\ \sin\theta_0}\left(\sqrt{2}\,r_1\ \sin\theta_0-\xi\right)H_0^{(1)}(k_1\xi)\mathrm{d}\xi \tag{47}$$

$$=4r_1^2\sin^2\theta_0\left(1+\frac{2\mathrm{i}}{\pi}\ln\frac{\gamma k_1 r_1\ \sin\theta_0}{\sqrt{2e^{3/2}}}\right)\quad .$$

Substituting Eq.(47) into Eq.(46) yields

$$\theta_0 r_1^{-\frac{1}{2}}\left\{A_{II}^0\cdot \mathrm{J}_\nu\left[2\sigma(gs)^{-\frac{1}{2}}r_1^{\frac{1}{2}}\right]+B_{II}^0\cdot \mathrm{Y}_\nu\left[2\sigma(gs)^{-\frac{1}{2}}r_1^{\frac{1}{2}}\right]\right\}+$$

$$\sum_{n=1}^{\infty} r_1^{-\frac{1}{2}}\left\{A_{II}^n\cdot \mathrm{J}_\nu\left[2\sigma(gs)^{-\frac{1}{2}}r_1^{\frac{1}{2}}\right]+B_{II}^n\cdot \mathrm{Y}_\nu\left[2\sigma(gs)^{-\frac{1}{2}}r_1^{\frac{1}{2}}\right]\right\}\cdot\frac{\sin(n\theta_0)}{n} \tag{48}$$

$$+\frac{\sigma\cdot G}{g}r_1\sin^2\theta_0\left(1+\frac{2\mathrm{i}}{\pi}\ln\frac{\gamma k_1 r_1\ \sin\theta_0}{\sqrt{2e^{3/2}}}\right)$$

$$=\theta_0 A_0^1 \mathrm{J}_0(k_1r_1)+\sum_{m=1}^{\infty}\frac{\sin n\theta_0}{n}A_n^1\mathrm{J}_n(k_1r_1)\quad .$$

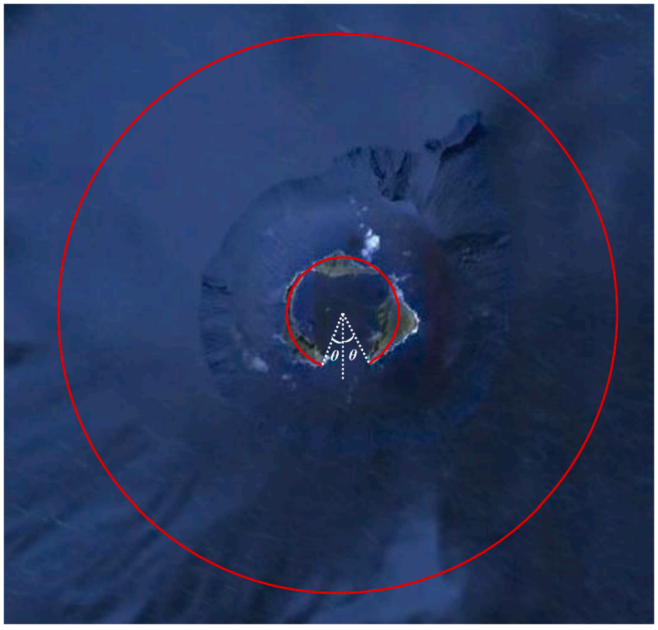

Fig. 1. A plan view of Maug Islands (from Google Earth).

As the radiated waves are limited to the harbor mouth, they can be neglected at the boundary line $r=r_2$. Thus, the matching condition Eq. (32) can be rewritten as

$$r_2^{-\frac{1}{2}}\left\{A_{II}^0\cdot \mathrm{J}_\nu\left[2\sigma(gs)^{-\frac{1}{2}}r_2^{\frac{1}{2}}\right]+B_{II}^0\cdot \mathrm{Y}_\nu\left[2\sigma(gs)^{-\frac{1}{2}}r_2^{\frac{1}{2}}\right]\right\}+$$

$$\sum_{n=1}^{\infty} r_2^{-\frac{1}{2}}\left\{A_{II}^n\cdot \mathrm{J}_\nu\left[2\sigma(gs)^{-\frac{1}{2}}r_2^{\frac{1}{2}}\right]+B_{II}^n\cdot \mathrm{Y}_\nu\left[2\sigma(gs)^{-\frac{1}{2}}r_2^{\frac{1}{2}}\right]\right\}\cos(n\theta) \tag{49}$$

$$=a_1\varepsilon_0\mathrm{J}_0(k_2r_2)+a_{\mathrm{III}}^0\mathrm{H}_0(k_2r_2)+$$

$$a_1\sum_{n=1}^{\infty}\mathrm{i}^n\varepsilon_n\mathrm{J}_n(k_2r_2)\cos n\theta+\sum_{n=1}^{\infty}a_{\mathrm{III}}^n\mathrm{H}_n(k_2r_2)\cos n\theta\quad ,$$

which yields

$$r_2^{-\frac{1}{2}}\left\{A_{II}^0\cdot \mathrm{J}_\nu\left[2\sigma(gs)^{-\frac{1}{2}}r_2^{\frac{1}{2}}\right]+B_{II}^0\cdot \mathrm{Y}_\nu\left[2\sigma(gs)^{-\frac{1}{2}}r_2^{\frac{1}{2}}\right]\right\} \tag{50}$$

$$=a_1\varepsilon_0\mathrm{J}_0k_2r_2+a_{\mathrm{III}}^0\mathrm{H}_0(k_2r_2)$$

and

$$r_2^{-\frac{1}{2}}\left\{A_{II}^n\cdot \mathrm{J}_\nu\left[2\sigma(gs)^{-\frac{1}{2}}r_2^{\frac{1}{2}}\right]+B_{II}^n\cdot \mathrm{Y}_\nu\left[2\sigma(gs)^{-\frac{1}{2}}r_2^{\frac{1}{2}}\right]\right\} \tag{51}$$

$$=a_1\mathrm{i}^n\varepsilon_n\mathrm{J}_n(k_2r_2)+a_{\mathrm{III}}^n\mathrm{H}_n(k_2r_2)\qquad \text{for}\ \ n\geq 1$$

Similar approach used in Eq.(33) gives

$$-\frac{1+\nu}{2}r_2^{-\frac{3}{2}}\left[A_0^{\mathrm{II}}\cdot J_\nu\left(\frac{2\sigma}{\sqrt{gs}}r_2^{\frac{1}{2}}\right)+B_0^{\mathrm{II}}\cdot Y_\nu\left(\frac{2\sigma}{\sqrt{gs}}r_2^{\frac{1}{2}}\right)\right]$$

$$+\frac{\sigma}{\sqrt{gs}}r_2^{-1}\left[A_0^{\mathrm{II}}\cdot J_{\nu-1}\left(\frac{2\sigma}{\sqrt{gs}}r_2^{\frac{1}{2}}\right)+B_0^{\mathrm{II}}\cdot Y_{\nu-1}\left(\frac{2\sigma}{\sqrt{gs}}r_2^{\frac{1}{2}}\right)\right] \tag{52}$$

$$=-a_1k_2\mathrm{J}_0(k_2r_2)+A_{\mathrm{III}}^0k_2\mathrm{H}_0(k_2r_2)\qquad \text{for}\quad n=0$$

and

$$-\frac{1+\nu}{2}r_2^{-\frac{3}{2}}\left[A_n^{\mathrm{II}}\cdot J_\nu\left(\frac{2\sigma}{\sqrt{gs}}r_2^{\frac{1}{2}}\right)+B_n^{\mathrm{II}}\cdot Y_\nu\left(\frac{2\sigma}{\sqrt{gs}}r_2^{\frac{1}{2}}\right)\right]$$

$$+\frac{\sigma}{\sqrt{gs}}r_2^{-1}\left\{A_n^{\mathrm{II}}\cdot J_\nu\left(\frac{2\sigma}{\sqrt{gs}}r_2^{\frac{1}{2}}\right)+B_n^{\mathrm{II}}\cdot Y_\nu\left(\frac{2\sigma}{\sqrt{gs}}r_2^{\frac{1}{2}}\right)\right\} \tag{53}$$

$$=2a_1\mathrm{i}^nk_2\mathrm{J}_{n-1}(k_2r_2)+2na_1\mathrm{i}^nr_2^{-1}\mathrm{J}_n(k_2r_2)+k_2A_{\mathrm{III}}^n\mathrm{H}_{n-1}(k_2r_2)$$

$$-nr_2^{-1}A_{\mathrm{III}}^n\mathrm{H}_n(k_2r_2)\qquad \text{for}\qquad n\geq 1\quad .$$

3. Comparison with existing analytical solutions

As shown in Fig. 2, when r_1 is very close to r_2 (i.e. h_1 becomes very close to h_2), the island will disappear and the topography will degenerate into a circular harbor of constant depth. Lee (1971) derived an analytical solution to investigate wave-induced oscillations inside harbors with arbitrary geometry and constant depth, and further conducted experiments to verify the theory.Fig. 1.

To reproduce the experiment of Lee (1971), the topographical parameters are adjusted to $r_1=0.228$ m and $r_2=0.229$ m, which leads to

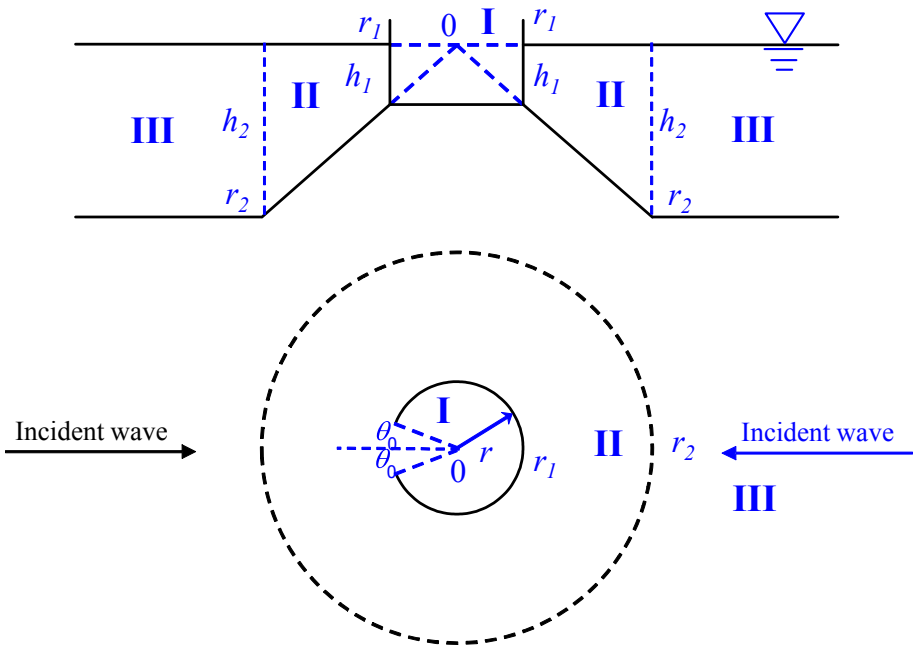

Fig. 2. Definition sketch of the circular harbor over a conical island.

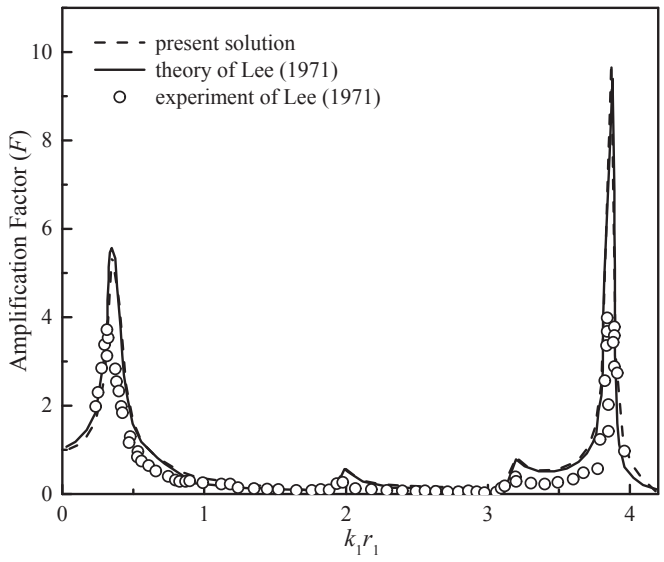

Fig. 3. Response curve of the circular harbor with a 10^0 opening at the center, where the radius of the harbor is $r = 0.228$ m and the water depth keeps constant as $h = 0.3$ m. The present solution respectively adopts $r_1 = 0.228$ m and $r_2 = 0.229$ m for the radii of the harbor and the island, which yields the water depth within the harbor is $h_1 = 0.3$ m and it is $h_2 = 0.301$ m in the open sea.

the water depth in the harbor $h_1 = 0.3$ m and the water depth in the open sea $h_2 = 0.301$ m. As the present solution is derived for the narrow harbor entrance, the results for the circular harbor with 10° opening are compared in Fig. 3. The amplification factor F, which is defined the ratio of the wave amplitude at any position inside the harbor to twice the incident wave amplitudes, is used to identify the response of a harbor to incident waves. The present solution agrees fairly well with that of Lee (1971). They share the same pattern and the values of the amplification factor are very close to each other. Since the energy dissipation arising from viscous effects and flow separation around the harbor entrance has not been considered in both theories, the analytical values of the peak amplification factor near resonance are obviously larger than the experimental values. However, the resonant frequencies and the variation patterns of the amplification factor curve shows good consistency between the experimental data and both theories.

On the other hand, when the mouth of the harbor is closed (i.e., the radiation waves from the harbor entrance are excluded), our solution degenerates into that for a cylindrical island over on a conical shoal. Zhu and Zhang (1996) have derived an analytical solution for the scattering waves around a cylindrical island mounted on a conical shoal in the open sea of constant depth. In order to compare with their results, the topographical parameters in their study are utilized, i.e., $r_1 = 10$ km, $h_1 = 1.33$ km and $h_2 = 4$ km. Two different values of r_2 (i.e., $r_2 = 200$ km and 80 km) are considered, which respectively correspond to $\gamma = 0.02$ and $\gamma = 0.05$ in the study of Zhu and Zhang (1996). The incident wave period is set to $T = 480$ s. Wave run-ups along the coastline of the cylindrical island for $\gamma = 0.02$ and $\gamma = 0.05$ are plotted in Fig. 4. The good agreement between two solutions indicates that the present analytic solution can well describe wave propagation over the island.

4. Oscillations within Maug Islands

The Maug Islands can be considered as a circular harbor with the radius of $r_1 = 1.1$ km and the constant water depth of $h_1 = 70$ m located over a conical island with the radius of $r_2 = 5.5$ km. It is surrounded by an open sea with the constant water depth of $h_2 = 350$ m. The opening of the harbor is $2\theta_0 = 10°$ and the constant slope of the island is $s = 0.0636$. As the narrow entrance assumption is satisfied in Fig. 3 by comparing the analytical solution with experiment results, the solution can be used confidently to examine the effect of the island on the harbor response to incident waves. In order to examine the effect of the island on the harbor response to incident waves, the oscillations in a circular harbor with the radius of $r = 1.1$ km and the constant water depth $h = 70$ m inside and outside are compared in Fig. 5. Regardless of whether the island exists or not, oscillations at the frequency of $\omega = 0.009$ rad/s are evident both at the center and the boundary positions with the angle $\theta = 45°$, 135° and 180° respectively. However, due to the shoaling effect of the underwater topography of the island on the incident waves, the resonant amplifications in the harbor located over the island shows to be larger than those without it. The frequencies of $\omega = 0.047$ rad/s and 0.076 rad/s are not obviously amplified by the harbor without the island and the corresponding amplification factors at these four positions are all less than 2.0, which indicates that they don't correspond to the resonant

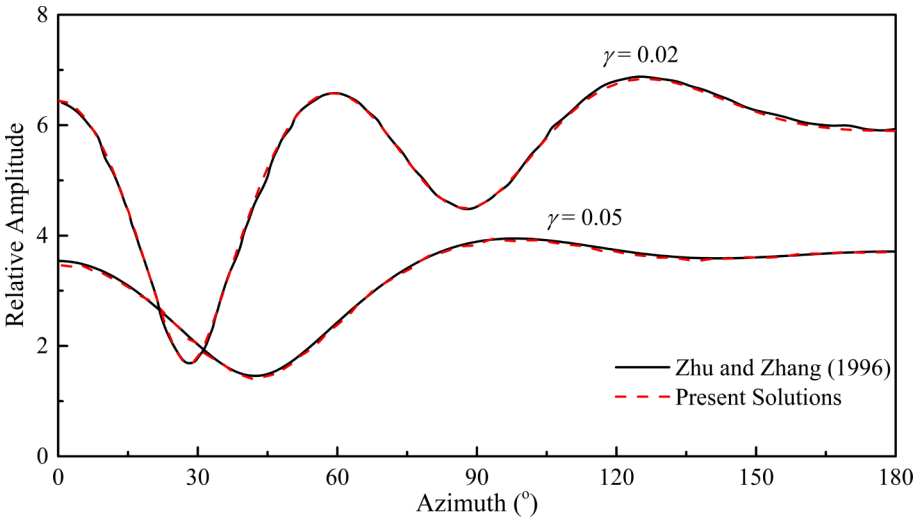

Fig. 4. Comparison of the present results for wave run-ups along the coastline of the cylindrical island with those of Zhu and Zhang (1996) for $T = 480$ s, $h_1 = 1.33$ km, $h_2 = 4$ km and $r_1 = 10$ km $\gamma = 0.02$ and 0.05 correspond to $r_2 = 200$ km and 80 km, respectively.

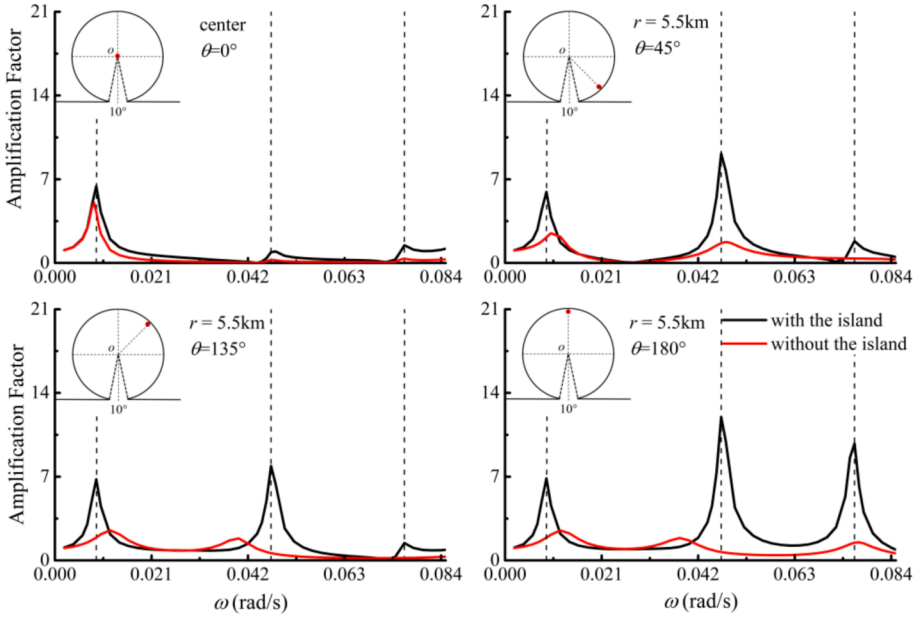

Fig. 5. Response curves of a 10°-opening circular harbors with and without the island at different locations. For the harbor over the island, $r_1 = 1.1$ km, $r_2 = 5.5$ km, $h_1 = 70$ m and $h_1 = 350$ m. For the harbor without the island, its radius is $r = 5.5$ km and the water depth inside and outside it is a constant of $h = 70$ m.

frequencies. On the contrary, the amplification factors at these two frequencies for the harbor located over the island can reach up to 12.0, an increase of more than 6 times, which should be due to the shoaling effect of underwater topography of the island.Fig. 6.

The distributions of relative wave amplitude for these three frequencies over the island and within the harbor are also presented in Fig. 5. As the wavelength of $\omega = 0.009$ rad/s is close to the radius of the island, the island cannot exert an obvious impact on the waves, which yields the relatively uniform distribution of wave amplitude over the island. The scattering effect of the island is enhanced with the increase of the wave frequency. The pattern of partial standing waves becomes more and more evident in front of the harbor. Furthermore, more wave energy is scattered laterally due to refraction and diffraction for these higher frequencies, and the scattering wave pattern over the island becomes more complicated.

The distributions of the wave amplitudes within the harbor are also shown to be distinct for different frequencies. The maximum and minimal values occur at different positions, and the nodal and antinodal lines present different geometric structures. For $\omega = 0.009$ rad/s, i.e. mode (0, 0) of the harbor, the amplitude is smallest at the entrance, and tends to increase gradually along the incident propagation direction and reaches the peak value at the backwall of the harbor. For $\omega = 0.047$ rad/s, i.e. mode (1, 0), a nodal line is observed approximately along $x = 0$, which symmetrically divides wave amplitude distribution inside the harbor into two parts. The maximum values are observed at the backwall together with the upper and lower sides of the entrance. For $\omega = 0.076$ rad/s, i.e. mode (2, 0), the wave amplitude distribution is almost evenly divided into four parts by two orthogonal nodal lines. The minimal value appears at the center, and the maximum values appear at the backwall, near the entrance and the up and down corners.

5. Conclusions

There are a number of harbors built over natural or artificial islands,

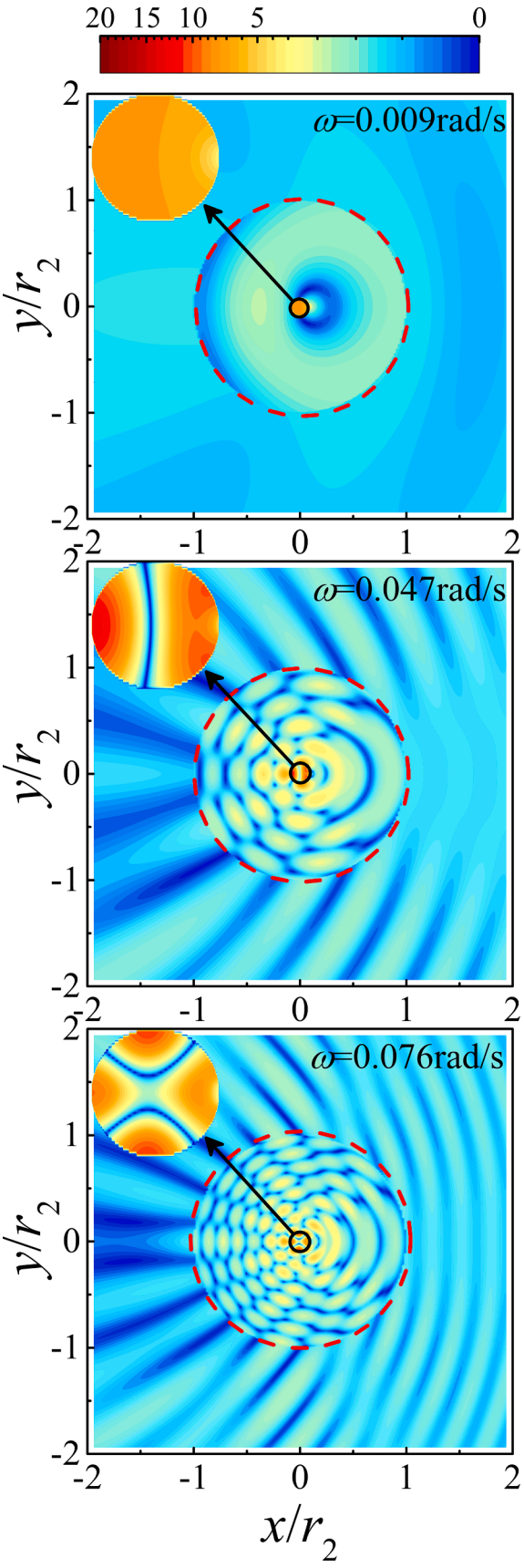

Fig. 6. Relative wave amplitude distribution around the simplified Maug Islands, i.e., a circular harbor with an opening of 10°, a radius of 1.1 km and a constant depth of 70 m located over a conical island with a radius of 5.5 km and a constant slope of 0.0636, where waves propagate from right to left.

and the incident waves from the open sea would be jointly affected by the island and the harbor. In order to reveal these features, an analytical solution for the wave oscillations within a circular harbor of constant depth over a conical island is derived. The domain of interest is divided into three regions, i.e., region I (within the harbor), region II (over the island) and region III (from the island toe to the deep sea). The free-surface elevation in the harbor of constant depth is described as a sum series of the first-kind Bessel function. Whereas the water depth varies linearly along the radial direction of the island in region II, the corresponding free-surface elevation is described as the combination of the first- and second-kind Bessel functions. In the open sea of constant depth, the incident and scattered waves are described with a Fourier-cosine series and a sum series of Hankel function, respectively. It is assumed that the width of the harbor entrance is very small compared to the incident wavelength, and furthermore, the island is so large that the radiated waves from the harbor entrance are rather small at the toe and can be ignored there. The final solution is obtained by matching the free-surface elevation and its derivative at the interfaces between the three regions. By adjusting the topographical parameters, the present analytical solution is used to predict the wave-induced oscillations in a circular harbor of constant depth and the scattering of long waves around a cylindrical island mounted on a conical shoal. The validity of the present analytical solution is fully proved via comparing the predicting results with the existing analytical solutions of Lee (1971) and Zhu and Zhang (1996).

As the topographical features of Maug Islands resembles the geometry studied in this article, the coupled oscillation characteristics for Maug Islands are examined. The distribution of wave amplitude over the island is highly related to both the topographical features and the incident wave frequency. For the effects of the topographical features, the existence of the island does aggravate oscillations in the harbor. The amplification factor is larger for a harbor over the island as compared to harbor without the island at the four positions. Moreover, the shoaling effect of underwater topography of the island on the incident waves shift some resonant frequencies. For the effects of the incident wave frequency, more complicated wave pattern appears over the island for the higher frequency due to wave refraction and diffraction. In addition, the wave amplitude distribution within the harbor also depends closely on the incident wave frequency via exciting different resonant modes. For different modes, the maximum and minimal values occur along with the nodal and anti-nodal lines displaying different geometric structures. The study is hoped to improve the understanding of oscillations in a harbor-island system and to provide preliminary estimates of resonance parameters.

Declaration ofcompeting interest

The authors declare that they have no known competing financial interests or personal relationships that could have appeared to influence the work reported in this paper.

Acknowledgements

This research was supported by the National Key Research and Development Program of China (No.: 2017YFC1404205), the National Natural Science Foundation of China (NO.: 51579090, 51609108) and the Fundamental Research Funds for the Central Universities (NO.: 2019B12214).

References

Cuomo, G., Guza, R.T., 2017. Infragravity seiches in a small harbor. J. Waterw. Port, Coast. Ocean Eng. 143 (5), 04017032.

Dong, G.-H., Wang, G., Ma, X.-Z., Ma, Y.-X., 2010. Harbor resonance induced by subaerial landslide-generated impact waves. Ocean Eng. 37 (10), 927–934.

Dong, G.-H., Wang, G., Ma, X.-Z., Ma, Y.-X., 2010. Numerical study of transient nonlinear harbor resonance. Sci. China Technol. Sci. 53 (2), 558–565.

Gao, J., Ji, C., Gaidai, O., Liu, Y., Ma, X., 2017. Numerical investigation of transient harbor oscillations induced by N-waves. Coast. Eng. 125, 119–131.
Jung, T.-H., Lee, C., Cho, Y.-S., 2010. Analytical solutions for long waves over a circular island. Coast. Eng. 57 (4), 440–446.
Kumar, P., Zhang, H., Yuen, D.A., Kim, K.I., 2013. Wave field analysis in a harbor with irregular geometry through boundary integral of Helmholtz equation with corner contributions. Comput. Fluids 88 (0), 287–297.
Lee, J.-J., 1971. Wave-induced oscillations in harbours of arbitrary geometry. J. Fluid Mech. 45 (02), 375–394.
Lee, J.-J., Lai, C.-P., Li, Y., 1998. Application of computer modeling for harbor resonance studies of Long Beach Los Angeles harbor basins. In: Proceedings of the 26th International Conference on Coastal Engineering. ASCE, Copenhagen, Denmark, pp. 1196–1209.
Ličer, M., Mourre, B., Troupin, C., Krietemeyer, A., Jansá, A., Tintoré, J., 2017. Numerical study of Balearic meteotsunami generation and propagation under synthetic gravity wave forcing. Ocean Model. 111, 38–45.
Liu, H.-W., Xie, J.-J., 2013. The series solution to the modified mild-slope equation for wave scattering by Homma islands. Wave Motion 50 (4), 869–884.
Losada, I.J., Gonzalez-Ondina, J.M., Diaz-Hernandez, G., Gonzalez, E.M., 2008. Numerical modeling of nonlinear resonance of semi-enclosed water bodies: description and experimental validation. Coast. Eng. 55 (1), 21–34.
Marcos, M., Monserrat, S., Medina, R., Lomonaco, P., 2005. Response of a harbor with two connected basins to incoming long waves. Appl. Ocean Res. 27 (4–5), 209–215.
Miles, J., Munk, W., 1961. Harbor paradox. J. Waterw. Harb. Div. 87 (3), 111–132.
Synolakis, C., 2003. Tsunami and seiche. In: Chen, W.-F., Scawthorn, C. (Eds.), Earthquake Engineering Handbook. CRC Press, Boca Raton, 9-1-90.
Thotagamuwage, D.T., Pattiaratchi, C.B., 2014. Influence of offshore topography on infragravity period oscillations in Two Rocks Marina, Western Australia. Coastal Engineering 91, 220–230. https://doi.org/10.1016/j.coastaleng.2014.05.011.
Vela, J., Pérez, B., González, M., Otero, L., Olabarrieta, M., Canals, M., Casamor, J.L., 2014. Tsunami resonance in palma bay and harbor, Majorca island, as induced by the 2003 Western Mediterranean earthquake. J. Geol. 122 (2), 165–182.
Wang, G., Dong, G.-H., Perlin, M., Ma, X.-Z., Ma, Y.-X., 2011. An analytic investigation of oscillations within a harbor of constant slope. Ocean Eng. 38, 479–486.
Wang, G., Dong, G.-H., Perlin, M., Ma, X.-Z., Ma, Y.-X., 2011. Numerical investigation of oscillations within a harbor of constant slope induced by seafloor movements. Ocean Eng. 38 (17–18), 2151–2161.
Wang, G., Fu, D., Zheng, J., Liang, Q., Zhang, Y., 2018. Analytic study on long wave transformation over a seamount with a pit. Ocean Eng. 154, 167–176.
Wang, G., Zheng, J.-H., Liang, Q.-H., Zheng, Y.-N., 2014. Analytical solutions for oscillations in a harbor with a hyperbolic-cosine squared bottom. Ocean Eng. 83 (0), 16–23.
Wijeratne, E.M.S., Woodworth, P.L., Pugh, D.T., 2010. Meteorological and internal wave forcing of seiches along the Sri Lanka coast. J. Geophys. Res. 115 (C3), C03014.
Zelt, J.A., Raichlen, F., 1990. A Lagrangian model for wave-induced harbour oscillations. J. Fluid Mech. 213, 203–225.
Zhang, Y.L., Zhu, S.P., 1994. New solutions for the propagation of long water waves over variable depth. J. Fluid Mech. 278, 391–406.
Zhu, S., Zhang, Y., 1996. Scattering of long waves around a circular island mounted on a conical shoal. Wave Motion 23 (4), 353–362.